Journal of The Electrochemical Society, **160** (6) H285-H293 (2013)
0013-4651/2013/160(6)/H285/9/31.00 © The Electrochemical Society

Cyclic Voltammetric Diagnostics for Inert, Uniform Density Films

Krysti L. Knoche,[a,*] Chaminda Hettige,[b,] Paul D. Moberg,[c] Sudath Amarasinghe,[d] and Johna Leddy[a,**,z]**

[a]*Department of Chemistry, University of Iowa, Iowa City, Iowa 52242, USA*
[b]*Oakland University, Rochester, Michigan 48309, USA*
[c]*Quicken Loans, Software Engineering, Fairfield, Iowa 52556, USA*
[d]*Ceramic Fuel Cells, Limited, SOFC, Noble Park, Victoria 3174, Australia*

Quantitative characterization of uniform density, electrochemically inert films on electrodes is achieved by cyclic voltammetry (CV) of a redox probe that partitions from electrolyte into the film. Electrochemically inert films generate no faradaic current in the voltammetric window of the probe. In simulation models, probes pre-equilibrate into films, electrolyze at electrodes, diffuse in film and solution, and extract across film solution interfaces. Film thickness is ℓ. Diffusion length δ approximates distance from the electrode where voltammetry perturbs probe concentration; $\delta \propto \nu^{-1/2}$ for scan rate ν. At high ν, $\delta < \ell$ and voltammetric morphologies are typical of semi-infinite linear diffusion. As ν slows, $\delta \gtrsim \ell$ and CV morphologies can change with relative probe flux in the film and solution. For higher solution flux, voltammograms assume sigmoidal (S-shaped) characteristics; higher film flux generates gaussian (thin layer CV) characteristics. For film and solution diffusion coefficients D_f and D_s and κ the equilibrium ratio of probe concentration in film to solution, diagnostics yield $\kappa\sqrt{(D_f/D_s)}$ and ℓ^2/D_f. Because diagnostics apply for all ν, films are fully parameterized by CV alone. Without these diagnostics, full characterization requires a second, steady state voltammetric measurement. Diagnostics are vetted with $[Ru(bpy)_3]^{2+}$ (probe) in inert polymer films of Nafion and of poly(styrenesulfonate).

Manuscript submitted January 9, 2013; revised manuscript received February 21, 2013. Published March 9, 2013. This was in part Paper 1560 presented at the San Francisco, California, Meeting of the Society, May 24–29, 2009.

Voltammetric characterization of polymer modified electrodes[1–15] established electrochemical methodology for characterization of films of all materials applied to electrodes. For polymer modified electrodes, electroactive films are defined as films where the redox active moieties are covalently bound to the polymer.[15] Electroinactive films do not contain covalently bound electroactive moieties and are electrochemically inert. Inert films include ion exchange polymers such as Nafion and poly(styrene sulfonate) that contain no covalently bound electroactive groups. Inert films themselves do not generate a voltammetric signal within the potential range of measurement. Under more restricted conditions, inert films can include electroactive films provided the voltammetric potential range does not electrolyze covalently bound electroactive species. Films include layers and coatings. Uniform density films have constant mass per volume throughout the thickness of the film.

To characterize a uniform density, electrochemically inert film on an electrode by cyclic voltammetry (CV), the film modified electrode is placed into an electrolyte that contains a redox probe and the probe extracts or permeates into the film and equilibrates prior to voltammetric perturbation. See Figure 1. During CV of the probe, the inert film impacts probe flux and is thereby reflected in the cyclic voltammetric morphology and current. In the CV potential window, the inert film itself remains electrochemically silent. Although CV is the most common method to characterize electrochemically inert films, diagnostics are not available to analyze data across all scan rates. Full characterization requires both CV and a steady state method such as rotating disk voltammetry (RDV). Use of transient and steady state voltammetry increases measurement uncertainty but is necessary because CV diagnostics are incomplete. Diffusion length δ approximates the distance from the electrode where the probe concentration is perturbed from its initial equilibrium value by voltammetric perturbation. δ is scan rate ν dependent as $\delta \propto \nu^{-1/2}$. Quantitative measurements by CV are limited to high ν where δ is less than the film thickness (ℓ) and diagnostics developed by Nicholson and Shain for semi-infinite linear diffusion apply.[16] Surprisingly, no diagnostics exist when ν slows and δ is comparable to ℓ. Given such diagnostics, CV alone characterizes uniform density, inert films; reduces experimental uncertainties; and simplifies characterization of films. Films include coatings, pharmaceutical drug delivery matrices, and modified electrodes that support sensors and catalyst layers.

Here, CV diagnostics are presented to parameterize inert films across all scan rates so that only CV is needed. Because coupled transient and steady state voltammetries are not required, statistical uncertainties introduced by the second voltammetry method are eliminated and soft films either not stable or distorted under hydrodynamic conditions can be evaluated. Diagnostics for CV of redox probes that permeate inert, thin films of uniform density are developed by computer simulation. The simulation is needed because available commercial voltammetric simulation software does not model the film solution interface well unless probe flux is limiting in either the film or solution. The one dimensional simulation is developed by well-established finite difference methods.[17–19] Boundary conditions for the film solution interface are imposed to ensure molewise conservation of material that moves across the interface. This is key to an effective simulation model of film modified electrodes.[20]

The computer model is for a macroscopic, planar electrode modified with a uniform density, inert film placed in a solution of redox probe. Probe extracts and pre-equilibrates in the film. See Figure 1. Under cyclic voltammetric perturbation, probe is electrolyzed at the electrode and diffuses to the electrode on the resulting concentration gradient. This establishes a probe concentration profile and δ that grows as time increases (ν decreases). Once δ reaches the film solution interface, probe extracts across the interface into the film and concentration of probe in the solution may be depleted as ν slows.

Voltammetric morphologies for film modified electrodes vary systematically with two parameters: relative flux in the film and solution and δ relative to ℓ. Responses range from the shape typical of reversible heterogeneous electron transfer and semi-infinite linear diffusion (hereafter referred to as avian) to the gaussian (bell curve) shape of thin layer voltammograms and to the sigmoidal (S-shaped curve) response of steady state voltammetry. The response is determined by the relative probe flux in the film and solution as the δ exceeds ℓ. The simulation yields voltammetric morphologies consistent with data in the literature. The simulated morphologies also illustrate that literature data may be misinterpreted as slow electron transfer kinetics, uncompensated resistance, or adsorption when the morphologies arise because of film properties. Dimensionless parameters characterize the morphologies. Diagnostic relationships between parameters and simulated current outputs allow experimentalists quantitative access to dimensionless parameter groups that embed diffusion coefficients, extraction parameter, and film thickness.

*Electrochemical Society Student Member.
**Electrochemical Society Active Member.
zE-mail: johna-leddy@uiowa.edu

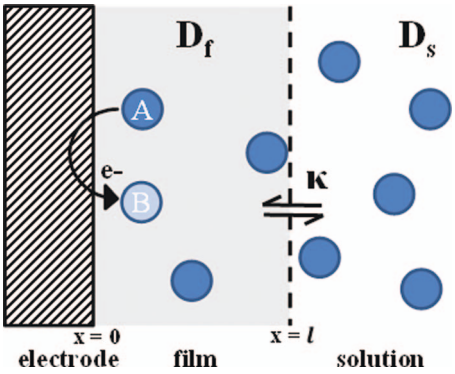

Figure 1. Redox probe A with concentration c^* and diffusion coefficient D_s in solution equilibrates into a uniformly dense film of thickness ℓ. In the film, A has diffusion coefficient D_f and concentration characterized with extraction parameter κ as κc^*. On voltammetric perturbation, A undergoes heterogeneous electron transfer at the electrode to become B. For the diagnostics, B has the same κ, D_f, and D_s as A and heterogeneous electron transfer is reversible.

Electrochemists tend to preserve discrete parameters of ℓ, extraction parameter κ, and diffusion coefficient in the film D_f, but modified electrodes are better characterized by parameter groups. Analytical solutions for transient chronoamperometric probe current at electrodes modified with inert films are fully characterized by only two dimensionless parameter groups $\sqrt{\ell^2/D_f t}$ and $\kappa\sqrt{D_f/D_s}$, where D_s is diffusion coefficient in solution.[21,22] Film thickness relative to diffusion length is characterized by $\sqrt{\ell^2/D_f t}$ and maximum sustainable flux in the film relative to solution is described by $\kappa\sqrt{D_f/D_s}$. Steady state methods yield inverse permeability, $\ell/\kappa D_f$, expressed in the ratio of $\sqrt{\ell^2/D_f}$ to $\kappa\sqrt{D_f/D_s}$. Inclusion of other experimental data such as film thickness allows evaluation of discrete parameters, but the parameter groups cannot be segregated into discrete ℓ, κ, and D_f by voltammetric methods alone. This does not arise through inadequacies of the CV simulation and analytical solutions for chronoamperometry, but rather reflects the fundamental, coupled processes that dictate transient voltammetric responses.

Diagnostics provide methodology to characterize films by CV alone. Diagnostics are developed for the same κ, D_f, and D_s for each the probe reactant and product, reversible heterogeneous electron transfer kinetics, and no homogeneous reactions. When CV is undertaken across scan rates that probe δ relative to ℓ, CV alone yields information equivalent to data from coupled electrochemical techniques of steady state RDV and high scan rate CV. The physical system, development of the simulation, simulated CV morphologies, and development of the diagnostics are presented. The diagnostics are presented in Equations 7 and 10.

The simulation and diagnostics (Equations 7 and 10) are vetted with experimental CV data for the redox probe tris(2,2′ -bipyridyl)dichlororuthenium(II) hexahydrate in Nafion and literature CV data for tris(2,2′ -bipyridyl)ruthenium(II) perchlorate in poly(styrene sulfonate). The redox cation is $[Ru(bpy)_3]^{2+}$ for both polymers. Nafion and poly(styrene sulfonate) are electrochemically inert polymers that form uniform density films.

The Physical System

Consider an electrode coated with a film of uniform density, as shown in Figure 1. ℓ is the thickness of the inert film in the electrolyte. In a solution of semi-infinite extent, probe A present in solution at concentration c^* (moles/cm^3) extracts into the film and A equilibrates in the film prior to voltammetric perturbation. In the film, equilibrium concentration of A is κc^*, where extraction parameter κ is the ratio of the equilibrium concentration in the film relative to the solution. Probe transports solely by diffusion in the solution and film with diffusion coefficients D_s and D_f (cm^2/s). Electrode area, A (cm^2), is sufficiently large that transport occurs in only one dimension. The coordinate normal to the electrode is x, where $x = 0$ at the electrode surface. Migration and local activity effects are not considered. The mathematical specification of the model is described in the Appendix and symbols are listed in the glossary.

On cyclic voltammetric perturbation, A is electrolyzed to B at the electrode film interface. The heterogeneous electron transfer reaction is characterized by a formal potential $E^{0'}$.

$$A + ne \rightleftharpoons B \qquad E^{0'} \qquad [1]$$

As A moves on the concentration gradient to the electrode, the concentration of A is depleted from its initial value. Diffusion length δ approximates the distance from the electrode where concentration of A differs from the initial condition. δ increases with time where $\delta \approx \sqrt{D_f t_k}$ where t_k is a time characteristic of voltammetric perturbation. For CV, $t_k = 1/nf\nu$ where $f = F/RT$.

The relationship between δ and ℓ determines how voltammograms are analyzed to characterize inert films. Historically, only data taken at scan rates sufficient to maintain the diffusion length within the film, $\delta < \ell$ are analyzed. When $\delta < \ell$, diagnostics appropriate to semi-infinite linear diffusion apply.[16] Cyclic voltammetric peak current i_p for reversible electron transfer kinetics is characterized by the Randles-Sevcik equation, where for an inert film and $\delta < \ell$, $i_p = 0.4463\sqrt{F^3/RT}n^{3/2}AD_f^{1/2}\kappa c^*\nu^{1/2}$. Data from a second method RDV are then combined with high ν CV to determine $\kappa\sqrt{D_f/D_s}$ and ℓ^2/D_f. Use of CV and RDV can increase errors if (1) the condition that $\delta < \ell$ for CV is not well met; (2) fragile films are not stable to shear of RDV; or (3) replicate but distinct films are used for CV and RDV.

Here, the CV simulation model includes $\delta \approx \ell$. Diagnostics are generated that allow use of all scan rate data so that data provided by CV alone is equivalent to that provided by steady state RDV plus CV when $\delta < \ell$.

Simulation Model Results

The CV simulation model yields a range of voltammetric morphologies, as shown in Figure 2. Dimensionless current $Z(E)$, a function of applied potential E, is the experimental current for the modified electrode made dimensionless with the known solution parameters.

$$Z(E) = \frac{i(t)\sqrt{t_k}}{nFAc^*\sqrt{D_s}} \qquad [2]$$

Morphologies include gaussian (bell curve) and sigmoidal (S curve) shapes. Morphologies consistent with semi-infinite linear diffusion and fast heterogeneous electron transfer are also apparent; in the interest of brevity, these morphologies are called avian. The morphologies other than avian arise as $\delta \approx \ell$ and are dependent on the relative probe flux in the film and solution. Avian responses are observed when flux in the film and solution are comparable. When film flux exceeds solution flux, morphologies assume gaussian characteristics, as found for voltammetry in thin layers where flux of probe is limited at the interface $x = \ell$. When solution flux exceeds film flux, a steady feed of probe to the film solution interface yields sigmoidal components, as found for steady state voltammetries.

In Figure 2, the heterogeneous electron transfer is modeled as reversible (Nernstian). Diagnostics are provided for fast electron transfer rates. The simulation, however, allows slower heterogeneous rates as modeled by Butler Volmer kinetics.[23]

Simulated cyclic voltammetric morphologies.— Voltammetric morphologies vary systematically with only two dimensionless parameters: ω relates flux in the film to flux in the solution and b relates the film thickness to diffusion length ($b \propto \nu^{1/2}$).

The term $\kappa\sqrt{D_f/D_s}$ characterizes flux in the film to flux in solution. (In the literature, the notation often includes $\gamma = \sqrt{D_s/D_f}$.) Let $x = \ell^-$ and $x = \ell^+$ be the positions immediately at the film solution interface on the film and solution sides respectively. The extraction

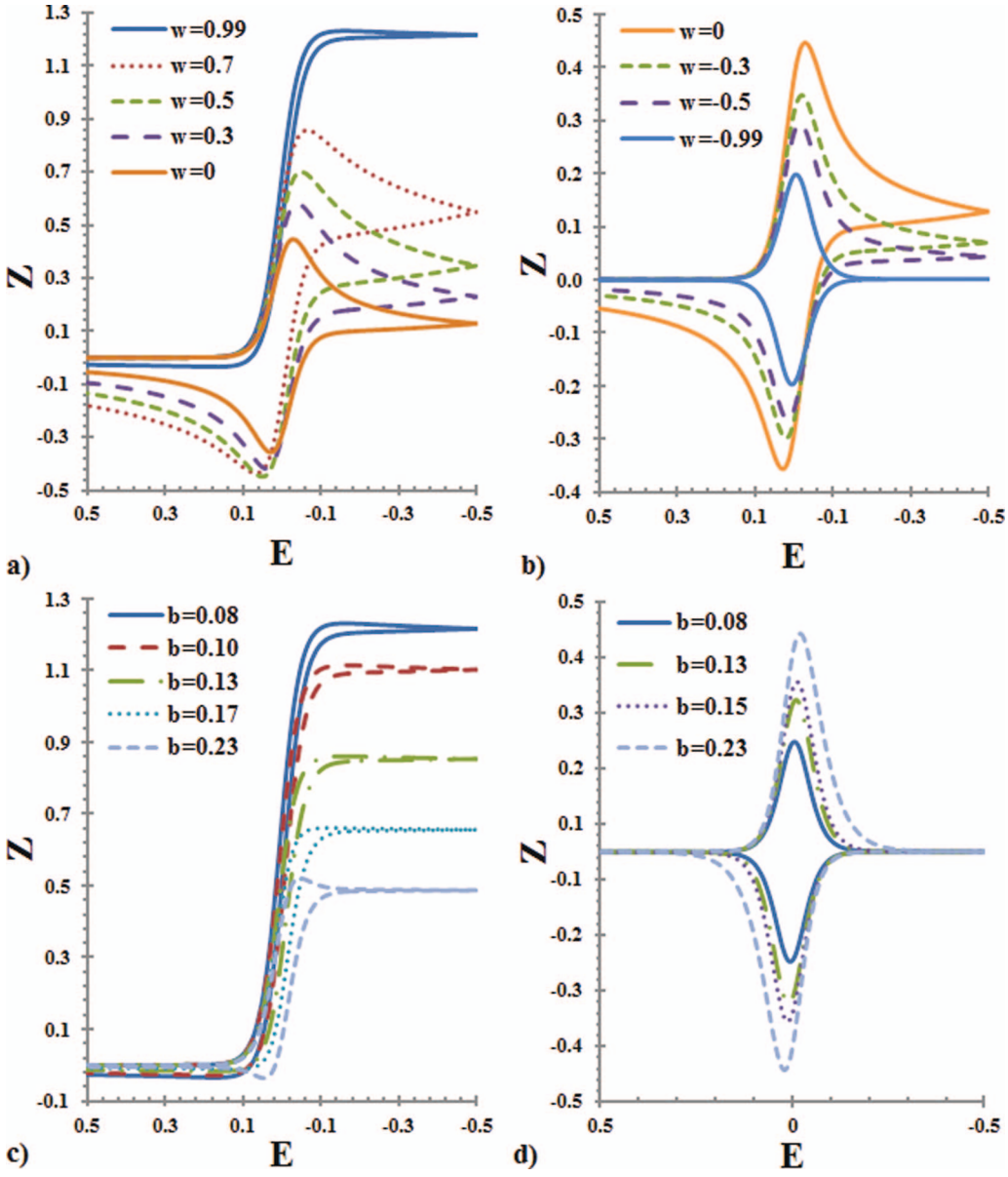

Figure 2. Simulated cyclic voltammograms expressed as dimensionless current $Z(E)$ for a range of $\omega = [1 - \kappa/\gamma]/[1 + \kappa/\gamma]$ and $b = \sqrt{\ell^2 nf\nu/D_f}$ values. a) For $b = 0.09$ ($\delta \gg \ell$) and $\omega \geq 0$, as ω increases, solution flux increases relative to film flux and morphology approaches sigmoidal as $c(\ell^+, t) \longrightarrow c^*$. b) For $b = 0.09$ and $\omega \leq 0$, as ω decreases, solution flux decreases relative to film flux and morphology approaches gaussian as $c(\ell^+, t) \longrightarrow 0$. When diffusion length is confined in the film ($b > 0.23$) morphology reverts to the avian morphology characteristic of linear diffusion. c) For the extreme $\omega = +0.99$ where flux in solution $\gg$ flux in the film and a range of scan rates $0.08 \leq b \leq 0.23$, the transition to steady state transport is mapped as b (and $\ell^2\nu$) decrease. d) For the extreme $\omega = -0.99$ where flux in solution $\ll$ flux in the film and a range of scan rates $0.08 \leq b \leq 0.23$, the transition to a gaussian response is mapped as b decreases. Note, normalizations of $Z(E)$ and b disallow immediate comparisons of relative experimental currents $i(E)$. Simulations were generated for reversible electron transfer kinetics. The diagnostics, based on the peak currents as a function of scan rate, determine both ω and ℓ^2/D_f from cyclic voltammetry alone.

parameter κ is the fixed ratio of concentrations in the film and solution at the interface, $\kappa = c_A(\ell^-, t)/c_A(\ell^+, t)$; also, $\kappa = c_{A,film}(t = 0)/c^*$, the ratio of equilibrium concentrations in the film and solution prior to voltammetric perturbation. The parameter ω found in analytical solutions for chronoamperometry[21,22] defines relative flux in the film and solution.

$$\omega = \frac{1 - \dfrac{\kappa\sqrt{D_f}}{\sqrt{D_s}}}{1 + \dfrac{\kappa\sqrt{D_f}}{\sqrt{D_s}}} \qquad -1 \leq \omega \leq 1 \qquad [3]$$

When flux in solution is large compared to the film, $\omega > 0$; when flux in solution is small compared to the film, $\omega < 0$; when flux in solution and the film are equal, $\omega = 0$. An advantage of ω as a parameter is that ω captures the full range of relative film and solution flux over a range limited between $+1$ and -1.

Because $t_k = 1/nf\nu$, ν sets $\delta \approx \sqrt{D_f t_k}$. Dimensionless b sets the ratio of film thickness ℓ to diffusion length δ. For b large, $\delta < \ell$.

$$b = \sqrt{\frac{\ell^2}{D_f t_k}} = \sqrt{\frac{\ell^2 nf\nu}{D_f}} \sim \frac{film\ thickness}{diffusion\ length} \qquad [4]$$

For each ω value, simulations were run for a set of b values to mimic δ well confined within the film ($b > 0.23$), δ comparable to ℓ ($0.08 \leq b \leq 0.23$), and δ extending well beyond ℓ ($b < 0.08$). As b (and ν) decrease, δ grows. The simulation outputs $Z(E)$ for a given ω

and b. Note that in Figure 2, the morphologies can be compared but the normalizations of $Z(E)$ and b do not immediately scale dimensionless $Z(E)$ as proportional to experimental current $i(E)$ for different values of ω and b.

For $\omega = 0$, cyclic voltammograms retain the avian shape characteristic of linear diffusion, as shown in Figure 2a and 2b. The voltammograms have dimensionless peak current $Z_{pf} = 0.4463$ and peak splittings (the potential difference for the forward and reverse peak currents) of $\Delta E_p = 57\ mV$, consistent with Nicholson and Shain's results.[16] For $\omega = 0$, flux in the film is equal to flux in solution, $\sqrt{D_s} = \kappa\sqrt{D_f}$, and the response is the same as that for an unmodified electrode.

For $\omega > 0$, solution flux is greater than film flux. In Figure 2a, voltammograms are shown for several values of $\omega \geq 0$ and $b = 0.09$ ($\delta \gg \ell$). As $\omega \rightarrow +1$, morphologies approach sigmoidal because film flux is sufficiently low that probe concentration at ℓ^+ is maintained near bulk concentration, $c(\ell^+, t) \rightarrow c^*$. This establishes a near linear concentration gradient across the film and the sigmoidal wave form characteristic of steady state transport results. Figure 2a maps the transition from avian morphology for $\omega = 0$ to the sigmoidal response as $\omega \rightarrow +1$.

For $\omega < 0$, film flux is higher than solution flux. In Figure 2b, voltammograms are shown for several values of $\omega \leq 0$ and $b = 0.09$ ($\delta \gg \ell$). As $\omega \rightarrow -1$, the cyclic voltammograms approach a gaussian shape because film flux is sufficiently high that solution flux is insufficient to maintain probe at ℓ^+ and $c(\ell^+, t) \rightarrow 0$. Depletion of probe at ℓ in the film yields the gaussian shape characteristic of thin layer voltammograms. Figure 2b maps the transition from avian morphology ($\omega = 0$) to a gaussian response as $\omega \rightarrow -1$. Note that $\omega < 0$ is most commonly generated by large κ because typically $D_f \lesssim D_s$. For polymer films, $\omega \longrightarrow -1$ most typically for ion exchange polymers.

Effects of varying b for fixed values of ω are shown in Figure 2c ($\omega = +0.99$) and Figure 2d ($\omega = -0.99$). This maps the transition between $\delta < \ell$ at $b = 0.23$, through $\delta \approx \ell$, to $\delta \gg \ell$ for $b = 0.08$. In Figure 2c ($\omega = +0.99$) as b decreases, the morphology transitions from a hummingbird-like shape to a sigmoid as a linear concentration profile is established in the film and $c(\ell^+, t) \longrightarrow c^*$. In Figure 2d ($\omega = -0.99$), the transition to a gaussian curve is mapped as b decreases $c(\ell^-, t) \longrightarrow 0$ and thin layer behavior is established.

These various simulation morphologies were generated for reversible heterogeneous electron transfer rates, where, for k^0 the standard heterogeneous electron transfer rate, $k^0 t_k \gg \delta$. On cursory inspection, some morphologies may appear similar to those for slow electron transfer at unmodified electrodes. If the probe is outer sphere and exhibits reversible morphologies when $\delta < \ell$ at high ν, then changes in the morphologies at slower ν when $\delta \gtrsim \ell$ are established by the film interface, not the electron transfer kinetics. A second note is that pinholes in a film will alter voltammetric morphologies. For a film with constant length and radius pinholes,[24] CV will exhibit avian morphology for $\delta < \ell$, morphology for slow electron transfer when $\delta \approx \ell$, and return to avian morphology when $\delta \gg \ell$. If scan rates are assessable for the full range of δ, then pinholes are readily discriminated from $\omega > 0$ because the evolution of voltammetric morphologies differs. If a full range of δ is not assessable, then quantitative evaluation of data under both the pinhole and uniform density film models will often identify the correct model.

Results of these studies are summarized as the forward sweep, dimensionless peak current Z_{pf} found for 11 values of ω each with 20 b-values. For sigmoidal waves as $\omega \rightarrow 1$, Z_{pf} is the maximum current. Some values are shown in Table I and all values are plotted in Figure 3 as $\ln Z_{pf}$ versus $-\ln b$.

Three domains of behavior are shown in Figure 3.

$b > 0.23$ When $b > 0.23$, $\ln Z_{pf}$ values converge to a single value for $-\ln(b) < 1$. This is consistent with a constant dimensionless peak current Z_{pf} for $\delta < \ell$ where the peak current expression for semi-infinite linear diffusion applies $i_{pf} = 0.4463 n^{3/2} AF\kappa c^* \sqrt{f D_f \nu}$. Then, $Z_{pf} = 0.4463$ and $\ln Z_{pf} = -0.8068$ as shown in the Table and Figure.

Table I. Tabulated values of dimensionless peak current Z_{pf} for $-0.99 \leq \omega \leq 0.99$ and $0.0050 \leq b \leq 2.0$.

	$Z_{pf}(\omega)$				
b	$\omega = 0.99$	$\omega = 0.50$	$\omega = 0$	$\omega = -0.50$	$\omega = -0.99$
0.005	1.2312	0.6962	0.4426	0.2927	0.1980
0.050	1.2314	0.6999	0.4463	0.2949	0.1980
0.090	1.2314	0.7000	0.4463	0.2949	0.1980
0.130	0.8609	0.5941	0.4463	0.3458	0.2734
0.170	0.6613	0.5296	0.4463	0.3834	0.3338
0.200	0.5717	0.4995	0.4463	0.4033	0.3677
0.500	0.4471	0.4467	0.4463	0.4459	0.4455
2.000	0.4463	0.4463	0.4463	0.4463	0.4463

$b < 0.08$ When $b < 0.08$, $\delta \gg \ell$ and Z_{pf} values are constant for a given ω, as shown in Figure 3 and Table I for $-\ln(b) > 2.5$. For $b = 0.050$ and $-0.7 \leq \omega \leq 0.7$, linear regression yields $\ln Z_{pf} = \ln[i_{pf}(n^{3/2} AFc^* \sqrt{f D_s \nu})^{-1}] = (0.87_2 \pm 0.01_3)\omega - (0.792_9 \pm 0.005_6)$ with $R^2 = 0.9985$. ω can be found from $\ln[i_{pf}/(n^{3/2} AFc^* \sqrt{f D_s \nu})] = 0.87\omega - 0.792$, but with less accuracy than the other methods. Note that when $\omega = 0$, this collapses to the result of Nicholson and Shain.[16]

$0.09 < b < 0.20$ For values of b where $\delta \approx \ell$, $\ln Z_{pf}$ varies linearly with $-\ln(b)$ for ω as shown in Figure 3 and Table I for $0.09 < b < 0.20$. As $|\omega|$ decreases from 1 toward 0, the magnitude of the slopes diminish and converge to zero as expected for $\omega = 0$. As tabulated in Table II, for each ω and twelve b-values between 0.09 and 0.20, regression of $\ln Z_{pf}$ with $-\ln b$ linearizes as

$$\ln Z_{pf} = -m \ln b + c \qquad [5]$$

where m and c depend linearly on ω. The regressions hold for $-0.99 \leq \omega \leq 0.99$. Regression yields $m = (0.86_0 \pm 0.02_2)\omega + (0.02_8 \pm 0.01_3)$, $R^2 = 0.994$ and $c = -(1.18_3 \pm 0.02_8)\omega - (0.84_1 \pm 0.01_6)$, $R^2 = 0.995$. This yields the final diagnostic that allows determination of ω and ℓ^2/D_f from CV alone.

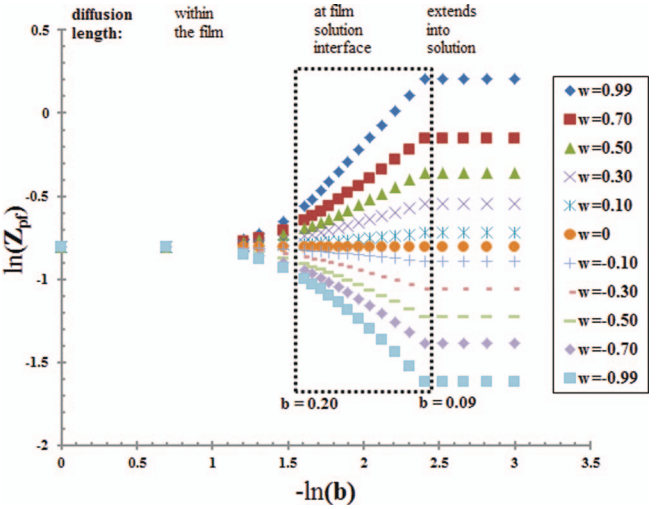

Figure 3. Plot of $\ln Z_{pf}$ versus $-\ln b$ where the dimensionless peak current, $Z_{pf} = i_{pf}/(nFAc^* \sqrt{nf\nu D_s})$. The dotted square encompasses the range of data used in the linearization, $0.09 \leq b \leq 0.20$. The range of behaviors established by δ relative to ℓ is noted at the top of the Figure.

Table II. Tabulated values of slope m, intercept c, and R^2 for lnZ_{pf} vs $-ln(b)$ for each ω and $0.09 \le b \le 0.2$.

ω	m	c	R^2
0.99	0.97189	− 2.1321	0.9998
0.7	0.62277	− 1.6570	0.9990
0.5	0.42895	− 1.3930	0.9986
0.3	0.25061	− 1.1497	0.9983
0.1	0.08185	− 0.9189	0.9979
0	− 0.00006	− 0.8066	0.9931
− 0.1	− 0.08075	− 0.6957	0.9975
− 0.3	− 0.23947	− 0.4768	0.9971
− 0.5	− 0.39602	− 0.2597	0.9966
− 0.7	− 0.55176	− 0.0423	0.9960
− 0.99	− 0.77851	0.2772	0.9949

Cyclic voltammetric diagnostics.— Cyclic voltammetric diagnostics are provided to extract both $\kappa\sqrt{D_f/D_s}$ and D_f/ℓ^2 for inert, uniform films from cyclic voltammetric forward peak currents i_{pf} recorded as a function of ν. These diagnostics are derived for $0.09 < b < 0.20$ and Equation 5 where substitution of the definitions of dimensionless parameters Z_{pf} and b yields

$$\ln \frac{i_{pf}\sqrt{t_k}}{nFAc^*\sqrt{D_s}} = -\ln\left[\frac{\ell^2}{D_f t_k}\right]^{\frac{m}{2}} + c \qquad [6]$$

where $t_k = 1/nf\nu$. Equation 6 is re-expressed in two ways to yield the diagnostics.

First, plot experimental $\ln i_{pf}$ versus $-\ln \nu$, which is linear when $0.09 < b < 0.20$.

$$\ln i_{pf} = -\left(\frac{m-1}{2}\right)\ln \nu + c - \frac{m}{2}\ln\left[\frac{\ell^2 nf}{D_f}\right] + \ln nFAc^*\sqrt{nfD_s} \qquad [7]$$

$$= -m' \ln \nu + c' \qquad [8]$$

This yields the experimental slope $m' = \frac{m-1}{2}$ and experimental intercept $c' = c - \frac{m}{2}\ln[\frac{\ell^2 nf}{D_f}] + \ln nFAc^*\sqrt{nfD_s}$. From m', ω is determined as $2m'+1 = m = (0.86_0 \pm 0.02_2)\omega + (0.02_8 \pm 0.01_3)$. From ω, $\kappa\sqrt{D_f/D_s} = (1-\omega)/(1+\omega)$. Once ω, m, c, and $nFAc^*\sqrt{nfD_s}$ are known, $\ln[\frac{\ell^2}{D_f}]$ can be extracted from c', but the errors will be larger.

Second, the antilog of Equation 6 reduces errors in determination of D_f/ℓ^2.

$$i_{pf}\exp(-c) = nFAc^*\sqrt{D_s}\left[\frac{D_f}{\ell^2}\right]^{\frac{m}{2}} t_k^{\frac{m-1}{2}} \qquad [9]$$

$$= nFAc^*\sqrt{D_s}\left[\frac{D_f}{\ell^2}\right]^{m'+\frac{1}{2}} t_k^{m'} \qquad [10]$$

From Equation 7, the slope m' of $\ln i_p$ versus $-\ln \nu$ yields m and ω that allows calculation of the constant $c = -(1.18_3 \pm 0.02_8)\omega - (0.84_1 \pm 0.01_6)$. A plot of i_{pf} versus $t_k^{m'}$ will yield a slope $m'' = \exp(c)nFAc^*\sqrt{D_s}[\frac{D_f}{\ell^2}]^{m'+\frac{1}{2}}$ and an intercept c'' of zero. Because $nFAc^*\sqrt{D_s}\exp(c)$ is known, $D_f/\ell^2 = [m''[nFAc^*\sqrt{D_s}\exp(c)]^{-1}]^{-(m'+\frac{1}{2})}$. The value of ℓ^2/D_f allows calculation of b and it should be verified that the scan rates used in the data analysis yield $0.09 \lesssim b \lesssim 0.20$.

Third, it is noted that ω can be found from each of the three domains of δ relative to ℓ and this serves as a check for self consistency in the analysis. (1) For short times and $\delta < \ell$, ($b > 0.23$), a plot of i_p versus $\nu^{1/2}$ yields a slope $0.4463n^{3/2}AF\kappa c^*\sqrt{fD_f}$ and an intercept of zero. To find ω, $\sqrt{D_s}$ is needed and is similarly found from a plot of i_p versus $\nu^{1/2}$ for the unmodified electrode. (2) For long times and $\delta \gg \ell$, ($b < 0.08$), ω can be found from $\ln[i_{pf}/(n^{3/2}AFc^*\sqrt{fD_s\nu})] = 0.87\omega - 0.792$ for $0.7 \ge \omega \ge -0.7$ but with lower accuracy. (3) For $\delta \approx \ell$, ($0.20 < b < 0.09$ and Equation 7), a plot of $\ln i_{pf}$ versus $-\ln \nu$ yields slope m' and thus ω. It should be verified that ω-values found in each range of δ are the same.

In summary, the advantage of these CV diagnostics is that D_f/ℓ^2 is found without additional voltammetric methods such as RDV. For $\delta \approx \ell$, ($0.20 < b < 0.09$), Equation 7 characterizes the plot of $\ln i_{pf}$ versus $-\ln \nu$ that yields a slope m' and thus ω. With m' and ω, c is determined and Equation 10 characterizes the plot of i_{pf} versus $t_k^{m'}$ that yields D_f/ℓ^2 from the slope because m' and $nFAc^*\sqrt{D_s}$ are known. Note that if ℓ is known, D_f and κ are separable. If diffusion is strictly by physical diffusion, D_f probes film viscosity (Stokes Einstein equation[23]).

Experimental Application

The diagnostics are tested on two systems. Experimental data collected for $[Ru(bpy)_3]^{2+}$ in Nafion films yield avian voltammograms (comparable film and solution flux). Literature cyclic voltammograms for $[Ru(bpy)_3]^{2+}$ in poly(styrene sulfonate) films exhibit gaussian morphologies (film flux greater than solution flux).[25]

Nafion film where $\omega > 0$.— The three electrode setup included a saturated calomel reference electrode (SCE) and platinum gauze counter electrode with a surface area at least 100 times larger than the working electrode. The aqueous solution contained 5.0 mM tris(2,2′ -bipyridyl)dichlororuthenium(II) chloride hexahydrate ($[Ru(bpy)_3]^{2+}$, Aldrich) and 0.50 M nitric acid (HNO_3, Fisher Scientific). A glassy carbon working electrode (Pine Instruments, $A = 0.452$ cm^2) was modified with a film of the electrochemically inert cation exchange polymer Nafion (DuPont) by pipet of 2.5 μL of 5 % w/v suspension of Nafion (Aldrich) onto the disk electrode. The film dried in air overnight. Films were then equilibrated in the electrolyte with probe for at least five hours and typically overnight. This was sufficient time to ensure full equilibration as shown by peak currents that were invariant after the equilibration period. Film thickness ℓ is estimated at 1.59 ± 0.05 μm given a density for Nafion in an acidic aqueous $[Ru(bpy)_3]^{2+}$ electrolyte of 1.98 ± 0.21 g/cm^3.[26] CV (CH Instruments 760B potentiostat) was performed over a potential window of 0.7 to 1.3 V vs SCE at $0.1 \le \nu \le 200$ mV/s with randomized scan rate order. Five separate films were analyzed on two similar electrodes. Triplicate data were collected for the unmodified glassy carbon electrodes to measure D_s. To verify $\kappa\sqrt{D_f}$, triplicate measurements were also made on a 6.0 μm Nafion film.

Data are shown in Figure 4 for CV of $Ru(bpy)_3^{2+}$ at 1.59 ± 0.05 μm Nafion film (solid lines) for $2 \le \nu \le 200$ mV/s with a 20 mV/s overlay at the same unmodified electrode (dashed line). For the Nafion film, voltammograms retain avian morphology at all scan rates. Based on Equation 7, a plot of $\ln i_{pf}$ versus $-\ln \nu$, as shown in Figure 5, yields a slope $m' = -0.46_7 \pm 0.01_1$ and intercept $c' = -7.5_3 \pm 0.05_3$ with an $R^2 = 0.997$. Analyses for the other four replicate films yielded values of m' and c' within 1.5 %. From m' and $2m'+1 = m = (0.86_0 \pm 0.02_2)\omega + (0.02_8 \pm 0.01_3)$, $\omega = 0.04_4 \pm 0.02_6$. From $\omega = 0.04_4 \pm 0.02_6$ and Equation 3, $\kappa\sqrt{D_f/D_s} = 0.92_0 \pm 0.04_0$. From unmodified electrode data, $D_s = (5.1_4 \pm 0.1_4) \times 10^{-6}$ cm^2/s, so that $\kappa\sqrt{D_f} = (2.0_9 \pm 0.04_1) \times 10^{-3}$ cm s$^{-1/2}$.

From Equation 10 and $m' = -0.46_7$, a plot of i_{pf} versus $t_k^{m'}$, as shown in Figure 6, yields slope $m'' = (1.0_3 \pm 0.01_3) \times 10^{-4}$, an intercept near zero as anticipated by Equation 10 of $c'' = (-4.5_2 \pm 1._7) \times 10^{-6}$, and $R^2 = 0.999$. From the slope m'', $D_f/\ell^2 = 0.97_6 \pm 0.02_6$ s^{-1}. Note that $m' + \frac{1}{2}$ approaches zero, so the uncertainty in D_f/ℓ^2 is large. For $\ell = 1.59$ μm, $D_f = (2.4_7 \pm 0.07_1) \times 10^{-8}$ cm^2/s. The value of D_f is relatively high. It is established that D_f in Nafion reflects transport by self exchange rather than simple physical diffusion.[27,22] The measured diffusion coefficient is all that is required for application of the model; diagnostics are appropriate for diffusion by hopping and physical diffusion.

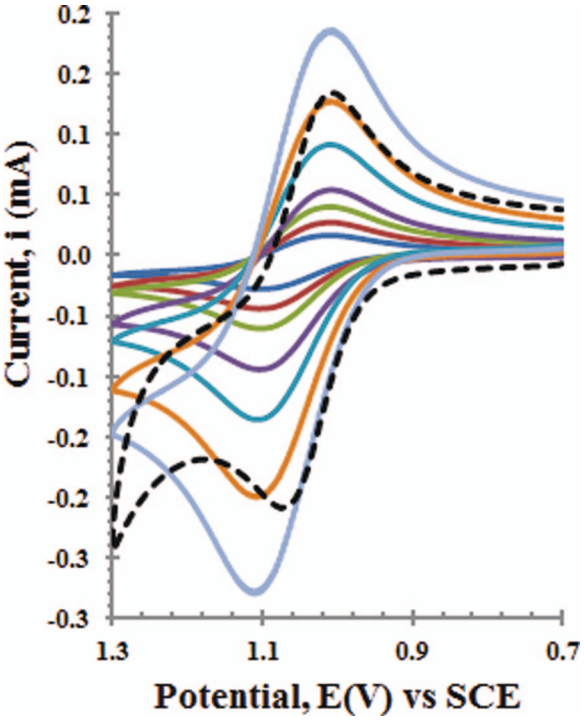

Figure 4. Cyclic voltammograms of 5.0 mM $[Ru(bpy)_3]^{2+}$ at a 1.59 $\pm$ 0.05 μm Nafion film on a glassy carbon electrode for scan rates 200, 100, 50, 20, 10, 5, and 2 mV/s, from largest current to smallest current respectively (solid lines). Overlaid is a voltammogram for the same conditions at an unmodified electrode at 20 mV/s (dotted line).

Given $D_f, \kappa\sqrt{D_f} = (2.09 \pm 0.04) \times 10^{-3}$ cm $s^{-1/2}$, $\kappa = 13._3 \pm 1._9$. Based on a maximum concentration of $[Ru(bpy)_3]^{2+}$ fully exchanged in Nafion of 0.9 M (from Nafion density (1.98 g/mL) and equivalent weight (1100 g/mol) for a dication) and solution concentration of 5.0 mM, $\kappa \leq 180$. From $\kappa = 13$, $[Ru(bpy)_3]^{2+}$ concentration in the film is less than fully exchanged, consistent with the proton rich (0.5 M HNO_3) electrolyte. In Nafion, the relative flux in the film and solution

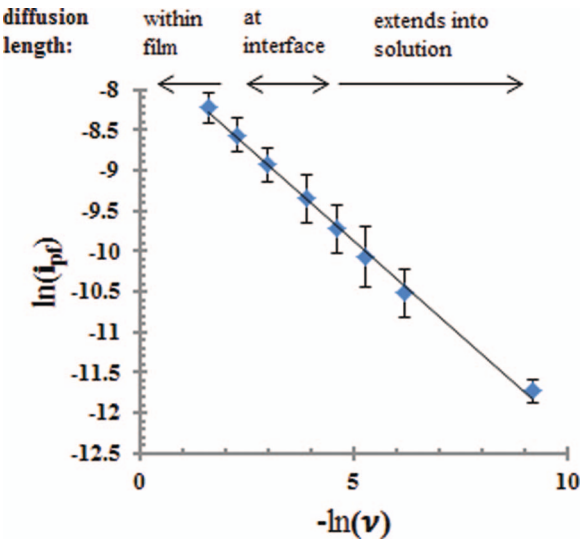

Figure 5. For experimental data in Figure 7, a plot of $\ln i_{pf}$ (A) against $-\ln \nu$ (V/s) is shown where regression yields $\ln i_{pf} = (-0.46_7 \pm 0.01_1) \ln \nu - (7.5_3 \pm 0.05_3)$ with regression coefficient $R^2 = 0.997$. This yields $\omega = 0.04_4 \pm 0.02_6$. Error bars are standard deviation for triplicate measurements of a single modified electrode.

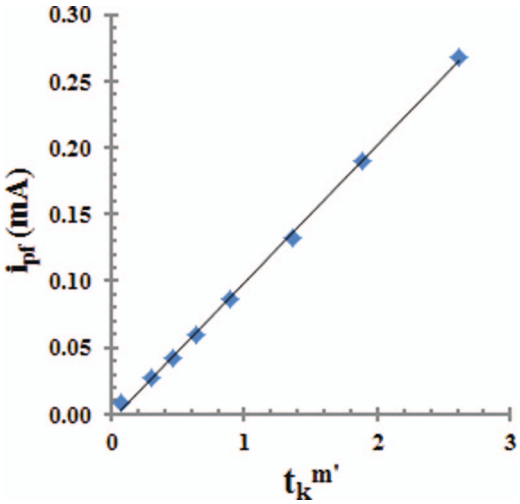

Figure 6. Plot of experimental data i_{pf} versus $t_k^{m'}$ for $[Ru(bpy)_3]^{2+}$ probe and 1.6 μm Nafion on a glassy carbon electrode. Regression yields $i_{pf} = (1.0_3 \pm 0.01_3) \times 10^{-4}[t_k^{m'}] - (4.5_2 \pm 1._7) \times 10^{-6}$ with regression coefficient $R^2 = 0.999$. Equation 10 yields $D_f/\ell^2 = 0.97_6 \pm 0.02_6$ s^{-1}.

will vary with κ, where the extraction parameter will vary with the relative charges, sizes, and concentrations of the probe and electrolyte. Given D_f, ℓ, and ν of 2, 5, 10, 20, 50, 100, and 200 mV/s, the b values are 0.535, 0.339, 0.239, 0.169, 0.107, 0.0757, and 0.0535. Relative uncertainties for calculated b values are ±0.03. From these values, δ for scan rates 2–10 mV/s are well into solution; for 20 and 50 mV/s, $\delta \approx \ell$; and for 100 and 200 mV/s, $\delta < \ell$. Regression is linear across across the full scan rate range because $\omega \longrightarrow 0$. For the 6 μm film, where $b = 3.48$, 2.20, 1.55, 1.10, 0.70, 0.49, and 0.35, $\delta < \ell$ at all ν and analysis by the Randles-Sevcik equation yields $\omega = 0.1_8 \pm 0.1_1$, a value consistent with the 1.59 μm films.

In Figure 7, fits to experimental voltammograms are simulated for $\omega = 0.044$ and b values for each scan rate. Fitting focused on the

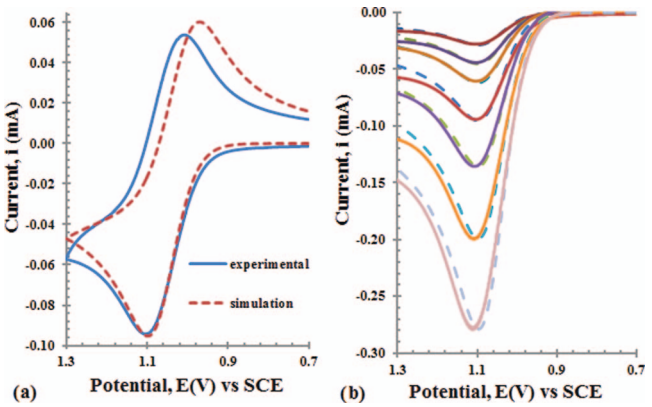

Figure 7. a) Experimental (solid) and simulated (dashed) CVs at 20 mV/s for 1.59 $\pm$ 0.05 μm Nafion film. Due to solvent electrolysis onset at about 1.2 V, only fit of the forward scan is of interest. Heterogeneous kinetics were included as $X0 = k^0\sqrt{t_k/D_f}$. The simulation used $\omega = 0.044$, $b = 0.0633$, $X0 = 4.0$, $\alpha = 0.45$. b) Experimental (solid) and simulation (dashed) forward waves for 2, 5, 10, 20, 50, 100, and 200 mV/s scan rates, from top to bottom. $\omega = 0.044$ and $\alpha = 0.45$ were used for all scan rates. Inputs of b and $X0$ varied only with ν. At 2 mV/s, $b = 0.0284$ and $X0 = 13$; at 5 mV/s, $b = 0.0450$ and $X0 = 8.0$; at 10 mV/s, $b = 0.0633$ and $X0 = 5.7$; at 20 mV/s, $b = 0.0899$ and $X0 = 4.0$; at 50 mV/s, $b = 0.142$ and $X0 = 2.5$; at 100 mV/s, $b = 0.201$ and $X0 = 1.8$; and at 200 mV/s, $b = 0.284$ and $X0 = 1.3$. The diffusion length is confined to the film for $b \geq 0.201$, which is $\nu \geq 100$ mV/s and $\delta \sim \ell$ for $0.0899 \leq b \leq 0.142$, $10 \leq \nu \leq 50$ mV/s.

forward scan oxidation wave because the onset of solvent electrolysis at about 1.2 V perturbed the baseline for the reverse wave. For 20 mV/s, a dimensionless standard heterogeneous rate constant of $X0 = k^0\sqrt{\frac{t_k}{D_f}} = 4.0$ and a transfer coefficient of $\alpha = 0.45$ fit the data. $k^0 \sim 0.0055$ cm/s. For the other scan rates, $X0$ was varied only to reflect change in t_k. The good quality of the fit is consistent with effective diagnostics. The model is based on uniform films that are pinhole free. Under cyclic voltammetric perturbation, pinholes manifest as sigmoidal waves once the diffusion length is comparable to the film thickness.[24] Here pinholes are not observed because waves are not sigmoidal and k^0 is invariant with scan rate.

Poly(styrene sulfonate) film where $\omega < 0$.— Well-documented CV data for poly(styrene sulfonate) films and the probe $[Ru(bpy)_3^{2+}]$ reported by Majda and Faulkner are characterized with the diagnostics.[25] A poly(styrene sulfonate) film of $\ell = 100 \pm 5$ nm was spin coated onto a platinum electrode ($A = 0.18$ cm^2) and placed in 0.5 mM tris(2,2′ -bipyridyl)ruthenium(II) perchlorate ($[Ru(bpy)_3]^{2+}$) and 0.1 M tetra-n-butylammonium tetrafluoroborate ($TBABF_4$) in 15 % methanol/acetonitrile. CVs between 0.0 to 1.2 V vs Ag | Ag^+ in acetonitrile at scan rates between 10 and 200 mV/s exhibit gaussian characteristics. The authors note that i_p vs v is linear over the range 10-100 mV/s and deviates negatively at higher scan rates.

From Equation 7, $\ln i_{pf}$ vs $-\ln v$ for $33 \leq v \leq 200$ mV/s yields slope $m' = -0.91_4 \pm 0.02_3$, intercept $c' = -6.7_6 \pm 0.06_1$, and $R^2 = 0.999$. From m', $\omega = -0.99_5 \pm 0.03_7$. $\kappa\sqrt{D_f/D_s} = 416 \pm 15$. The diffusion coefficient in solution $D_{s(MeCN)} = (1.3_3 \pm 0.1_4) \times 10^{-5}$ cm^2/s was estimated with Walden's rule $D_1\eta_1 = D_2\eta_2$ given the diffusion coefficient of $[Ru(bpy)_3]^{2+}$ in water $D_{s(H_2O)} = (5.1_4 \pm 0.1_4) \times 10^{-6}$ cm^2/s as determined here, viscosity of water $\eta_{(H_2O,25^\circ C)} = 0.890$ cP, and viscosity of acetonitrile $\eta_{(MeCN,25^\circ C)} = 0.343$ cP. From Equation 10, a plot of i_{pf} versus $t_k^{m'}$ yields slope $m'' = (4.0_0 \pm 0.07_7) \times 10^{-7}$ and an intercept approaching zero of $c'' = (2.4_4 \pm 2.9_7) \times 10^{-6}$ with $R^2 = 0.999$. From the slope, $D_f/\ell^2 = (1.4_7 \pm 0.04_3) \times 10^3$ and, for $\ell = 100$ nm, $D_f = (1.4_6 \pm 0.08_0) \times 10^{-7}$ cm^2/s such that $\kappa = (3.9_7 \pm 0.2_6) \times 10^3$.

The gaussian CV morphology is consistent with $\omega \longrightarrow -1$ that arises from high κ, and the relatively high D_f. Faulkner and Majda discuss the high extraction parameter in the paper and estimate a maximum concentration in the film of 1.4×10^{-3} mol/cm^3. For the reported solution concentration $c^* = 5 \times 10^{-7}$ mol/cm^3, $\kappa = 2800$, which is comparable to the found κ of 4000. Given $D_f = (1.46 \pm 0.08) \times 10^{-7}$ cm^2/s, scan rates 10, 20, 33, 50, 100, and 200 mV/s convert to b values of 0.209, 0.148, 0.115, 0.0937, 0.066, and 0.0468 (with relative uncertainties ± 0.03), such that for 10 to 50 mV/s δ is at the film solution interface, and at 100 and 200 mV/s, $\delta < \ell$, consistent with the analysis. Pinholes are not of concern for gaussian morphologies.

Conclusions

The model and diagnostics address a long standing question in voltammetric analysis of how to extract characteristic film parameters as the diffusion length of a redox probe exceeds the thickness of an inert, uniform film. Cyclic voltammetric morphologies are fully characterized by two parameters: ω compares probe flux in the film to the solution and b relates film thickness to diffusion length. When diffusion length is well established in solution (b is small) and ω differs from zero, cyclic voltammograms deviate from the avian shape characteristic of semi-infinite linear diffusion in a single phase. When $\omega \rightarrow +1$, film flux is low, concentration at the film solution interface approaches c^*, and a linear concentration profile is established in the film such that steady state transport established in the film yields a sigmoidal voltammogram. When $\omega \rightarrow -1$, film flux is sufficiently high that the solution cannot feed probe to the interface at a sufficient rate and the concentration of probe at ℓ^+ drops to zero such that concentration in the film is depleted and a gaussian voltammogram typical of a thin layer results. Because data are evaluated across scan rates that drive diffusion lengths out of the film, films are characterized by CV alone. Here, experimental and literature data are analyzed according to the diagnostics and verified by simulation with $\kappa\sqrt{D_f}$ found from ω and ℓ^2/D_f from b.

Acknowledgments

The support of the National Science Foundation is gratefully acknowledged (NSF 0809745).

Appendix: Simulation Details

The mathematical specification of the model and distinct details of the simulation are presented. For effective simulation, precise specification of flux across the film solution interface is necessary and molewise conservation of probe is required.

Mathematical Specification

The model shown in Figure 1 is specified mathematically. The one dimensional diffusion equation (Fick's second law) applies for film and solution. $c(x, t)$ is the concentration of probe at distance x from the electrode at time, t. For probe within the film $0 \leq x \leq \ell$ and diffusion coefficient D_f,

$$\frac{\partial c(x,t)}{\partial t} = D_f \frac{\partial^2 c(x,t)}{\partial x^2} \qquad 0 \leq x \leq \ell \qquad [A1]$$

For solution, $x > \ell$ and D_s,

$$\frac{\partial c(x,t)}{\partial t} = D_s \frac{\partial^2 c(x,t)}{\partial x^2} \qquad x > \ell \qquad [A2]$$

For the reaction $A + ne \rightleftharpoons B$, expressions of $c(x, t)$ are applicable for the reactant A and product B as $c_A(x, t)$ and $c_B(x, t)$. For c^* the bulk and initial concentration of probe A in the solution and κ the extraction parameter, the two initial conditions for reactant A and product B are:

$$c_A(x, 0) = \kappa c^* \qquad 0 \leq x \leq \ell \qquad [A3]$$

$$c_A(x, 0) = c^* \qquad x > \ell \qquad [A4]$$

$$c_B(x, 0) = 0 \qquad 0 \leq x \leq \ell \qquad [A5]$$

$$c_B(x, 0) = 0 \qquad x > \ell \qquad [A6]$$

Four boundary conditions are applied: one condition each for the film and the solution and two conditions for the film solution interface. For the solution,

$$\lim_{x\to\infty} c_A(x, t) = c^* \qquad [A7]$$

$$\lim_{x\to\infty} c_B(x, t) = 0 \qquad [A8]$$

At the film solution interface, the concentrations are governed by equilibrium and the same κ for A and B.

$$c_A(\ell^-, t) = \kappa c_A(\ell^+, t) \qquad [A9]$$

$$c_B(\ell^-, t) = \kappa c_B(\ell^+, t) \qquad [A10]$$

where $c(\ell^-, t)$ and $c(\ell^+, t)$ are probe concentrations immediately at the interface on the film and solution sides, respectively. Also, for each A and B, flux of probe from solution must equal the flux of probe into the film.

$$D_f \frac{dc(x,t)}{dx}\bigg|_{x=\ell^-} = D_s \frac{dc(x,t)}{dx}\bigg|_{x=\ell^+} \qquad [A11]$$

At the electrode film interface, $x = 0$, the voltammetric perturbation determines the boundary condition.

Butler Volmer kinetics describe the potential E dependent forward (reduction) $k_f(E)$ and backward (oxidation) $k_b(E)$ heterogeneous electron transfer rates for $A + ne \rightleftharpoons B$ with formal potential $E^{0'}$ and standard heterogeneous rate constant k^0 (cm/s).

$$k_f(E) = k^0 \exp\left[-\frac{\alpha nF}{RT}(E - E^{0'})\right] \qquad [A12]$$

$$k_b(E) = k^0 \exp\left[\frac{(1-\alpha)nF}{RT}(E - E^{0'})\right] \qquad [A13]$$

Diagnostics are provided for facile heterogeneous electron transfer where $k^0[D_f/t_k]^{1/2} \geq 50,000$, but the simulation can be used to fit data when the kinetics are slower. Flux of A to the electrode must equal flux of B away from the electrode and is set by $k_f(E)$ and $k_b(E)$ and surface concentrations of A and B.

$$D_f \frac{\partial c_A(x,t)}{\partial x}\bigg|_{x=0} = -D_f \frac{\partial c_B(x,t)}{\partial x}\bigg|_{x=0} \quad [A14]$$

$$= k_f(E)\, c_A(0,t) - k_b(E)\, c_B(0,t) \quad [A15]$$

The time dependent current, $i(t)$, is set by the flux of A to the electrode of area A. For cyclic voltammetry, $i(E)$ is used because E varies linearly with time at scan rate ν (V/s).

$$\frac{i(t)}{nFA} = D_f \frac{\partial c_A(x,t)}{\partial x}\bigg|_{x=0} \quad [A16]$$

Comments on Simulation Protocols

The model is expressed as a dimensionless, explicit finite difference simulation, as described in the literature.[17–19] Space and time are uniformly discretized and assigned counters j and k, respectively. Simulation parameters are dimensionless ratios of system parameters. Precise simulation of this system requires rigorous, molewise conservation of A and B at the film solution interface. Diffusion coefficients D_f and D_s differ, yet flux across the film solution interface must be conserved (Equation A11) while equilibrium is maintained (Equation A9). Moles of probe that move out of the solution must equal the moles of probe that move into the film. Molewise conservation is developed analogously to expressions for flux and electron transfer kinetics at the electrode electrolyte interface. For diffusion in a bulk phase, fractional probe concentration $f(j,k)$ and dimensionless diffusion coefficient $\mathbb{D}$ yield the well known expression

$$f(j,k+1) = f(j,k) + \mathbb{D}[f(j+1,k) - 2f(j,k) + f(j-1,k)] \quad [A17]$$

At the film solution interface, spatial coordinate $\mathbb{L}$ is the last space element in the film and $\mathbb{L}+1$ is the first space element in the solution, and $\mathbb{D}_f$ and $\mathbb{D}_s$ are the dimensionless diffusion coefficients in film and solution. Concentrations are measured in the middle of the spatial element but boundary conditions in Equations A9 and A11 are specified at the edge of the element immediately at the interface, $c(\ell^-,t)$ and $c(\ell^+,t)$. Application of the boundary conditions and linearization of the concentration gradients to express $c(\ell^-,t)$ and $c(\ell^+,t)$ in terms of $f(\mathbb{L},k)$ and $f(\mathbb{L}+1,k)$ modifies Equation A17, as detailed in reference.[20] $\gamma = \sqrt{D_s/D_f} = \sqrt{\mathbb{D}_s/\mathbb{D}_f}$.

$$f(\mathbb{L},k+1) = f(\mathbb{L},k) + \frac{\mathbb{D}_f}{\kappa+\gamma^2}\left\{\begin{array}{c} 2\kappa\gamma^2 f(\mathbb{L}+1,k) \\ -(\kappa+3\gamma^2)f(\mathbb{L},k) + (\kappa+\gamma^2)f(\mathbb{L}-1,k)\end{array}\right\} \quad [A18]$$

$$f(\mathbb{L}+1,k+1) = f(\mathbb{L}+1,k) + \frac{\mathbb{D}_s}{\kappa+\gamma^2}\left\{\begin{array}{c} (\kappa+\gamma^2)\, f(\mathbb{L}+2,k) \\ -(3\kappa+\gamma^2)\, f(\mathbb{L}+1,k) + 2f(\mathbb{L},k)\end{array}\right\} \quad [A19]$$

The validity of the simulation is established by, first, verification that the output of the simulation does not change with further increases in the spatial and temporal resolution, and, second, comparison of the simulated output to known limits cases of semi-infinite linear and thin layer diffusion.

For the simulation outputs and diagnostics provided here, the values of each κ, D_f, and D_s are the same for A and B; the number of boxes in the film $\mathbb{L} = 20$; and the number of time steps $k_{max} = 1 \times 10^5$. In the simulation code, all parameters can be varied.

Glossary of Symbols

ℓ	film thickness (cm)
ℓ^-	immediately on the film side of the film solution interface
ℓ^+	immediate on the solution side of the film solution interface
κ	extraction parameter, ratio of the equilibrium concentration of the probe in the film relative to the solution
δ	diffusion length, distance from the electrode surface where the concentration differs from the equilibrium concentration under voltage perturbation, $\delta \approx \sqrt{D_f t_k}$ when $\delta \lesssim \ell$ (cm)
x	distance from the electrode surface (cm)
t	time since the start of the voltage perturbation (s)
$c(x,t)$	concentration (moles/cm^3) as a function of distance x and time t
c^*	bulk concentration (moles/cm^3)
D_f	diffusion coefficient in the film (cm^2/s)
D_s	diffusion coefficient in solution (cm^2/s)
γ	dimensionless ratio $\sqrt{D_s/D_f}$
υ	scan rate (V/s)
i	measured current (A)
i_{pf}	peak current on the forward sweep (A)
Z	dimensionless current, $Z(E) = i(E)/nFAc^*\sqrt{D_s nf\upsilon}$
Z_{pf}	dimensionless peak forward current $Z_{pf} = i_{pf}/nFAc^*\sqrt{D_s nf\upsilon}$
ΔE_p	peak splitting, difference in potential for the forward and reverse peak currents (V)
t_k	dimensionless time, $t_k = [nf\upsilon]^{-1}$
$k_f(E)$	potential dependent heterogeneous reduction rate (cm/s)
$k_b(E)$	potential dependent heterogeneous oxidation rate (cm/s)
k^0	standard heterogeneous rate constant at $E^{0'}$ (cm/s)
α	transfer coefficient for heterogeneous electron transfer
ω	dimensionless parameter comparing relative flux in the film and solution $\omega = [1-\kappa\sqrt{D_f/D_s}][1+\kappa\sqrt{D_f/D_s}]^{-1}$ where $-1 \leq \omega \leq +1$
b	dimensionless parameter comparing diffusion length and film thickness $b = [\ell^2/D_f t_k]^{1/2}$
E	potential applied to the electrode (V)
$E^{0'}$	formal potential for the reaction $A + ne \rightleftharpoons B$ (V)
F	Faraday constant
R	gas constant
T	temperature (K)
$f = F/RT$ (V^{-1})	
n	number of electrons transferred
A	area of the electrode (cm^2)

Simulation Parameters

j	simulation space counter
k	simulation time counter
k_{max}	total number of time increments
$f(j,k)$	simulation dimensionless fractional concentration as a function of dimensionless space and dimensionless time
$\mathbb{D}_f$, $\mathbb{D}_s$	simulation dimensionless diffusion coefficients
$\mathbb{L}$	simulation film thickness (number of space increments in film)

References

1. K. Snell and A. Keenan, *Chem. Soc. Rev.*, **8**, 259 (1979).
2. R. Murray, *Acc. Chem. Res.*, **13**, 135 (1980).
3. R. Murray, in *Electroanalytical Chemistry, A Series of Advances*, A. Bard, Editor, Vol. 13 Marcel Dekker, Inc., New York, (1984) 191–368.
4. R. Murray, *Ann. Rev. Mat. Sci.*, **14**, 145 (1984).
5. L. Faulkner, *Chem. Eng. News*, **62**, 28 (1984).
6. H. Abruna, *Coord. Chem. Rev.*, **86**, 135 (1986).
7. A. Hillman, in *Electrochemical Science and Technology of Polymers*, R. Linford, Editor, Vol. 1 Elsevier, London, (1987) 103–292.
8. M. Kaneko and D. Worhle, *Adv. Polym. Sci.*, **84**, 141 (1988).
9. A. Merz, *Top. Curr. Chem.*, **152**, 49 (1990).
10. M. Lyons, *Annu. Rep. Prog. Chem., Sect. C*, **87**, 119 (1990).
11. I. Rubinstein, Electrochemical Processes at Polymer-Coated Electrode, in *Applied Polymer Analysis and Characterization*, J. Mitchell, Editor, Vol. II Hanser, New York, (1991) 233–258.
12. R. Murray, *Molecular Design of Electrode Surfaces* Vol. 22 of *Techniques of Chemistry* Interscience, New York, (1992).
13. R. Forster and J. Vos, in *Analytical Voltammetry*, M. Smyth and J. Vos, Editors, Vol. 27 Elsevier, Amsterdam, (1992) 465–529.
14. R. Mortimer, in *Research in Chemical Kinetics*, R. Compton and G. Hancock, Editors, Vol. 2 Elsevier, Amsterdam, (1994) 261–311.
15. A. J. Bard and L. R. Faulkner, in *Electrochemical Methods*, John Wiley & Sons, New York, (2001) p 580–631.
16. R. Nicholson and I. Shain, *Anal. Chem.*, **36**, 706 (1964).
17. S. W. Feldberg, in *Computers in Chemistry and Instrumentation*, J. Mattson, H. Mark, and H. MacDonald, Editors, Marcel Dekker, Inc., New York, (1972) Chapter 7.
18. A. J. Bard and L. R. Faulkner, in *Electrochemical Methods*, John Wiley & Sons, Inc., New York, (1980) p 675–698.
19. J. Maloy, in *Laboratory Techniques in Electroanalytical Chemistry*, P. Kissinger and W. Heineman, Editors, Marcel Dekker, Inc., New York, (1984) 417–462.
20. C. Hettige, *Characterization and Models for Uniform and Non-uniform Films on Electrodes*, Ph.D.thesis, University of Iowa, 2007.

21. P. Peerce and A. Bard, *J. Electroanal. Chem.*, **112**, 97 (1980).
22. H. S. White, J. Leddy, and A. J. Bard, *J. Am. Chem. Soc.*, **104**, 4811 (1982).
23. A. Bard and L. Faulkner, *Electrochemical Methods* John Wiley & Sons, Inc., New York, (2001) Second ed.
24. C. Amatore, J. Saveant, and D. Tessier, *J. Electroanal. Chem.*, **147**, 39 (1983).
25. M. M. Majda and L. R. Faulkner, *J. Electroanal. Chem.*, **169**, 77 (1984).
26. K. Oberbroeckling, D. Dunwoody, S. Minteer, and J. J. Leddy, *Anal. Chem.*, **74**, 4797 (2002).
27. D. A. Buttry and F. C. Anson, *J. Am. Chem. Soc.*, **105**, 685 (1983).